

## Article

# Self-Healable and Recyclable Biomass-Derived Polyurethane Networks through Carbon Dioxide Immobilization

Seohyun Baek <sup>†</sup>, Juhyen Lee <sup>†</sup>, Hyunwoo Kim, Inhwon Cha and Changsik Song <sup>\* ID</sup>

Department of Chemistry, Sungkyunkwan University, Suwon 16419, Korea; backgo04@gmail.com (S.B.); wngusqq@naver.com (J.L.); khw2651@naver.com (H.K.); ddrfgt@hotmail.com (I.C.)

\* Correspondence: songcs@skku.edu

† These authors contributed equally to this work.

**Abstract:** Due to growing environmental issues, research on carbon dioxide (CO<sub>2</sub>) use is widely conducted and efforts are being made to produce useful materials from biomass-derived resources. However, polymer materials developed by a combined strategy (i.e., both CO<sub>2</sub>-immobilized and biomass-derived) are rare. In this study, we synthesized biomass-derived poly(carbonate-co-urethane) (PCU) networks using CO<sub>2</sub>-immobilized furan carbonate diols (FCDs) via an ecofriendly method. The synthesis of FCDs was performed by directly introducing CO<sub>2</sub> into a biomass-derived 2,5-bis(hydroxymethyl)furan. Using mechanochemical synthesis (ball-milling), the PCU networks were effortlessly prepared from FCDs, erythritol, and diisocyanate, which were then hot-pressed into films. The thermal and thermomechanical properties of the PCU networks were thoroughly characterized by thermogravimetric analysis, differential scanning calorimetry, dynamic (thermal) mechanical analysis, and using a rheometer. The self-healing and recyclable properties of the PCU films were successfully demonstrated using dynamic covalent bonds. Interestingly, transcarbamoylation (urethane exchange) occurred preferentially as opposed to transcarbonation (carbonate exchange). We believe our approach presents an efficient means for producing sustainable polyurethane copolymers using biomass-derived and CO<sub>2</sub>-immobilized diols.

**Keywords:** biomass; carbon dioxide; covalent adaptive network

**Citation:** Baek, S.; Lee, J.; Kim, H.; Cha, I.; Song, C. Self-Healable and Recyclable Biomass-Derived Polyurethane Networks through Carbon Dioxide Immobilization. *Polymers* **2021**, *13*, 4381. <https://doi.org/10.3390/polym13244381>

Academic Editor: Arantxa Eceiza Mendiguren

Received: 23 November 2021

Accepted: 11 December 2021

Published: 14 December 2021

**Publisher's Note:** MDPI stays neutral with regard to jurisdictional claims in published maps and institutional affiliations.



**Copyright:** © 2021 by the authors. Licensee MDPI, Basel, Switzerland. This article is an open access article distributed under the terms and conditions of the Creative Commons Attribution (CC BY) license (<https://creativecommons.org/licenses/by/4.0/>).

## 1. Introduction

Due to global warming and environmental pollution, research on the use of carbon dioxide (CO<sub>2</sub>) is broadly conducted alongside efforts to reduce carbon emissions via CO<sub>2</sub> capture and storage [1–5]. This relatively inert gas can be efficiently converted into polymerizable platforms (monomers) and polymers, as well as many commodity chemicals such as methanol, carboxylic acid, and dimethyl carbonate [6–8]. For example, 5 or 6-membered cyclic carbonates, which can undergo ring-opening polymerizations, have been prepared by ring-closing reactions of 1,2 or 1,3-diols (or their equivalents) with CO<sub>2</sub> [9–12], or by the cycloaddition of CO<sub>2</sub> to ethylene oxide and other oxiranes [13–16]. Direct copolymerization methods (i.e., CO<sub>2</sub> as a comonomer) have also been developed, e.g., ring-opening copolymerization with oxirane monomer(s) [17–19], and step-growth polymerizations with diols or dihalides [2,20]. However, synthesizing polymer or polymer platforms from biomass-based materials by directly introducing CO<sub>2</sub> is rare. Although some biomass-derived oxiranes or aliphatic alcohols (diols) will be compatible with the conversion reaction or direct copolymerization of CO<sub>2</sub> [21,22], furan-based biomass-derived monomers, such as 5-(hydroxymethyl)furfural (HMF) and 2,5-bis(hydroxymethyl)furan (BHMF) have not been utilized in CO<sub>2</sub> immobilization.

Biomass feedstocks are ecofriendly and sustainable alternative resources and include forestry and crop residues, algae, municipal, and other organic wastes that can be used directly as fuel or converted into other reusable forms [23–26]. For example, cellulosic biomass can be converted into alcohols and acids, such as HMF, 2,5-furandicarboxylic

acid, and isosorbide, from which various ecofriendly polymers can be synthesized [27–29]. Other lignocellulosic sugar alcohols, such as sorbitol, mannitol, xylitol, and erythritol, are also potential fuels and chemicals that are widely used in ecofriendly polymers and pharmaceutical applications [30–36]. We aimed to develop furan carbonate diols (FCDs) by directly immobilizing CO<sub>2</sub> into furan-based, biomass-derived diols such as BHMF (Figure 1). These FCDs could then be further utilized to produce urethane-based network polymers, i.e., poly(carbonate-co-urethane) (PCU) networks. To the best of our knowledge, there are no prior reports on the production of network polyurethane copolymers using biomass feedstock and CO<sub>2</sub> simultaneously.

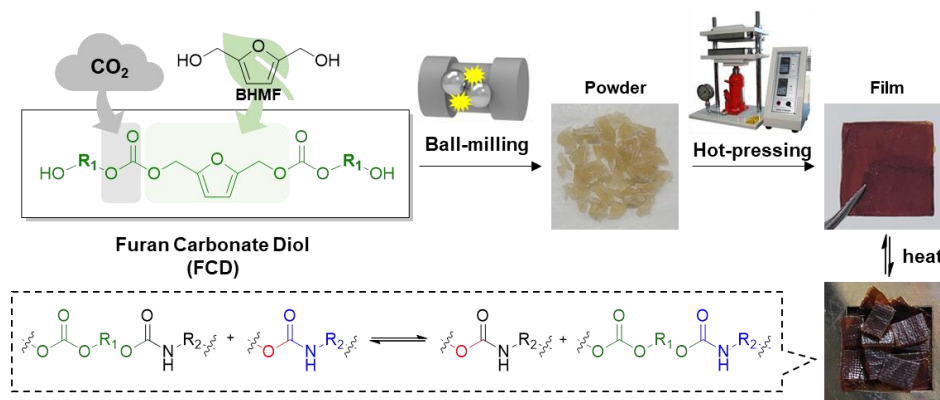


**Figure 1.** Synthesis of ecofriendly CO<sub>2</sub>-immobilized poly(carbonate-co-urethane) (PCU) networks and the preparation of the PCU films using a hot press.

Network polyurethanes (NPU) are generally synthesized from a polyol as a network structure and have many applications because of their good elastic properties, thermal stability, and solvent resistance [37–40]. However, conventional NPUs are thermosets and cannot be recycled. Interestingly, these NPUs (and other network polymers) can acquire malleability and recyclability using covalent-bond (i.e., urethane) exchange reactions. Such network polymers are broadly defined as covalent adaptable networks (CANs) and enabled by dynamic covalent chemistry (DCC) such as transesterification, transcarbonation (carbonate exchange), transcarbamoylation (urethane exchange), and silyl ether exchange [41–44]. Generally, CANs are known to operate through two types of mechanisms, i.e., dissociative and associative processes [45,46]. Dissociative CANs can be depolymerized in thermal equilibrium states and then repolymerized, which may result in the loss of their crosslinking density and mechanical modulus. Conversely, associative CANs continuously maintain their crosslinking density under thermal equilibrium during a dynamic bond exchange. Research on the development of CANs using biomass-based monomers is actively being conducted [47,48], providing reprocessable, recyclable, and self-healable polymer networks through DCC [48–50]. However, cases of CANs using a biomass-based, CO<sub>2</sub>-immobilized platform are rare.

In this study, we prepared biomass-derived urethane-based network polymers using a FCD, a new platform derived from the direct immobilization of CO<sub>2</sub> into BHMF [2,51–53]. The synthesized PCU network polymers were fabricated into films (Figure 1) and their thermal and thermomechanical properties were thoroughly characterized. Using a model compound study, we demonstrated that the thermally-induced reprocessing and self-healing properties of the PCU films arose due to the dynamic covalent exchange of urethane bonds, rather than carbonates. We believe our strategy using the simultaneous use of biomass and CO<sub>2</sub> will be useful for the development of sustainable polymer materials.

## 2. Materials and Methods

### 2.1. Materials

All chemicals used in the experiments were purchased from commercial sources: 2,5-bis(hydroxymethyl)furan (Nanjing Sunshine Chemical Co., Ltd., Nanjing, China), 6-Bromo-1-hexanol (TCI, Tokyo, Japan), 3-Bromo-1-propanol (Sigma Aldrich, St. Louis, MO, USA), 1,4-Benzenedimethanol (TCI, Tokyo, Japan), tert-Butyl(chloro)diphenylsilane (Sigma Aldrich, St. Louis, MO, USA), imidazole (Alfa Aesar, Ward Hill, MA, USA), erythritol (TCI, Tokyo, Japan), hexamethylene diisocyanate (TCI, Tokyo, Japan), 4,4'-diisocyanatomethylenedicyclohexane (TCI, Tokyo, Japan), cesium carbonate (TCI, Tokyo, Japan), tetrabutylammonium fluoride (Alfa Aesar, Ward Hill, MA, USA), dibutyltin dilaurate (TCI, Tokyo, Japan), ammonium chloride (Samchun Chemical, Seoul, Korea), sodium sulfate (Samchun Chemical, Seoul, Korea), all solvents including dichloromethane, N-methyl-2-pyrrolidone, tetrahydrofuran, ethyl acetate, dimethyl sulfoxide, dimethylformamide (Samchun Chemical, Seoul, Korea) and deuterated solvents for nuclear magnetic resonance (Cambridge Isotope Laboratories, Tewksbury, MA, USA).

### 2.2. Methods

#### 2.2.1. Synthesis of Furan Carbonate Diols Protected with Tert-Butyldiphenylsilane (FCD-Ps)

The weighed protected  $\omega$ -hydroxy bromoalkane (TBDPSO-R<sub>1</sub>-Br; P1~3) (P1 185 mg; P2 166 mg; P3 193 mg, 2.2 eq, 0.44 mmol) was transferred to an autoclave using a dichloromethane (DCM), and the DCM was removed using a vacuum. The BHMf (26 mg, 0.20 mmol), cesium carbonate (Cs<sub>2</sub>CO<sub>3</sub>; 261 mg, 0.80 mmol), and N-methyl-2-pyrrolidone (NMP; 0.50 mL) were consecutively added; the autoclave was then sealed and pressurized with CO<sub>2</sub> to 10 bar. The resulting reaction mixture was stirred at 100 °C for 24 h. After the reaction, the autoclave was cooled to 25 °C and the CO<sub>2</sub> was released. The product was purified using silica gel flash column chromatography (10% ethyl acetate in hexanes) to provide FCD-Ps as a colorless oil.

FCD-P1: R<sub>1</sub> = hexylene. Yield 77 mg (43%). <sup>1</sup>H NMR (500 MHz, DMSO-*d*<sub>6</sub>):  $\delta$  (ppm): 7.60 (m, 8H), 7.43 (m, 12H), 6.54 (s, 2H), 5.08 (s, 4H), 4.05 (t, *J* = 6.35 Hz, 4H), 3.62 (t, *J* = 6.35 Hz, 4H), 1.56 (m, 8H), 1.34 (m, 8H), 0.98 (s, 18H). <sup>13</sup>C NMR (125 MHz, DMSO-*d*<sub>6</sub>):  $\delta$  (ppm): 154.70, 150.20, 135.47, 133.80, 130.23, 128.31, 112.63, 68.22, 63.73, 61.11, 32.25, 31.17, 28.49, 27.13, 25.27, 19.23.

FCD-P2: R<sub>1</sub> = propylene. Yield 86 mg (53%). <sup>1</sup>H NMR (500 MHz, DMSO-*d*<sub>6</sub>):  $\delta$  (ppm): 7.59 (m, 8H), 7.42 (m, 12H), 6.56 (s, 2H), 5.09 (s, 4H), 4.24 (t, *J* = 6.15 Hz, 4H), 3.69 (t, *J* = 5.95 Hz, 4H), 1.85 (t, *J* = 6.05 Hz, 4H), 0.97 (s, 18H). <sup>13</sup>C NMR (125 MHz, DMSO-*d*<sub>6</sub>):  $\delta$  (ppm): 154.63, 150.16, 135.43, 133.44, 130.31, 128.34, 112.72, 65.13, 61.17, 60.19, 31.38, 27.04, 19.21.

FCD-P3: R<sub>1</sub> = *p*-xylylene. Yield 14 mg (8%). <sup>1</sup>H NMR (500 MHz, DMSO-*d*<sub>6</sub>):  $\delta$  (ppm): 7.64 (m, 8H), 7.45 (m, 12H), 7.36 (s, 8H), 6.57 (s, 2H), 5.15 (s, 4H), 5.13 (s, 4H), 4.77 (s, 4H), 1.03 (s, 18H). <sup>13</sup>C NMR (125 MHz, DMSO-*d*<sub>6</sub>):  $\delta$  (ppm): 154.57, 150.13, 141.34, 135.46, 134.47, 133.29, 130.42, 128.79, 128.43, 126.36, 112.78, 69.53, 65.26, 61.38, 27.11, 19.33.

#### 2.2.2. Synthesis of the Furan Carbonate Diols (FCDs)

To a solution of FCD-P (0.074 mmol) in anhydrous THF (0.80 mL), tetrabutylammonium fluoride (TBAF; 1.0 M in THF, 0.16 mL, 0.16 mmol) was added at room temperature under N<sub>2</sub>. The mixture was stirred for 3 h at room temperature, quenched with a saturated aqueous ammonium chloride solution, and extracted with ethyl acetate (EtOAc  $\times$  3). The combined organic layers were dried over anhydrous sodium sulfate, filtered, and concentrated in vacuo. The residue was purified by flash silica gel column chromatography (3:1 hexanes/EtOAc) to afford FCD as a colorless oil.

FCD-1: R<sub>1</sub> = hexylene. Yield 29 mg (95%). <sup>1</sup>H NMR (500 MHz, DMSO-*d*<sub>6</sub>):  $\delta$  (ppm): 6.55 (s, 2H), 5.09 (s, 4H), 4.34 (t, *J* = 5.05 Hz, 2H), 4.08 (m, 4H), 3.37 (m, 4H), 1.58 (m, 4H), 1.40 (m, 4H), 1.29 (m, 8H). <sup>13</sup>C NMR (125 MHz, DMSO-*d*<sub>6</sub>):  $\delta$  (ppm): 154.24, 149.72, 112.17,

67.83, 60.65, 32.34, 28.11, 25.08, 24.70. FTIR ( $\text{cm}^{-1}$ ): 3379 (O–H stretching vibration), 1745 (C=O stretching vibration), 1248 (C–O–C stretching vibration).

FCD-3:  $R_1 = p$ -xylylene. Yield 5 mg (15%).  $^1\text{H}$  NMR (500 MHz,  $\text{DMSO-}d_6$ ):  $\delta$  (ppm): 7.38 (m, 4H), 7.32 (m, 4H), 6.56 (s, 2H), 5.21 (t,  $J = 5.75$  Hz, 2H), 5.13 (m, 10H), 4.50 (d,  $J = 5.5$  Hz, 2H).  $^{13}\text{C}$  NMR (125 MHz,  $\text{DMSO-}d_6$ ):  $\delta$  (ppm): 154.52, 150.11, 136.01, 128.76, 128.60, 126.94, 112.81, 69.28, 63.04, 61.42. FTIR ( $\text{cm}^{-1}$ ): 3330 (O–H stretching vibration), 1743 (C=O stretching vibration), 1236 (C–O–C stretching vibration).

### 2.2.3. Synthesis of the Poly(Carbonate-co-Urethane) Networks (PCUs) via Ball-Milling

FCD-1 (416 mg, 1.0 mmol) or FCD-3 (456 mg, 1.0 mmol), erythritol (122 mg, 1.0 mmol), hexamethylene diisocyanate (HDI; 504 mg, 3.0 mmol) or 4,4'-diisocyanato-methylenediclohexane (HMDI; 787 mg, 3.0 mmol), and dibutyltin dilaurate (DBTDL; 1.0 mol%) were added in a 25 mL stainless steel vessel with two stainless steel balls (diameter, 15 mm each). The mixture was mounted on a mixer and vibrated at 20 Hz for 60 min. The product obtained was a yellow solid. FTIR ( $\text{cm}^{-1}$ ): 3344 (N–H stretching vibration), 2262 (N=C=O stretching vibration), 1725 (C=O stretching vibration), 1246 (NH–C=O stretching vibration).

### 2.2.4. Fabrication of the PCU Films

The synthesized PCU was dispersed in dimethyl sulfoxide (DMSO) at a concentration of 10 wt%. The solution was transferred to a polytetrafluoroethylene (PTFE) Teflon mold (30 × 30 mm, 10 mm thickness), and the solvent was dried in an oven at 70 °C for 12 h. The dried sample was transferred to a stainless steel plate (12 × 12 mm, 0.8 mm thickness) and hot-pressed at 120 °C for 6 h. FTIR ( $\text{cm}^{-1}$ ): 3344 (N–H stretching vibration), 1725 (C=O stretching vibration), 1246 (NH–C=O stretching vibration).

## 2.3. Measurements

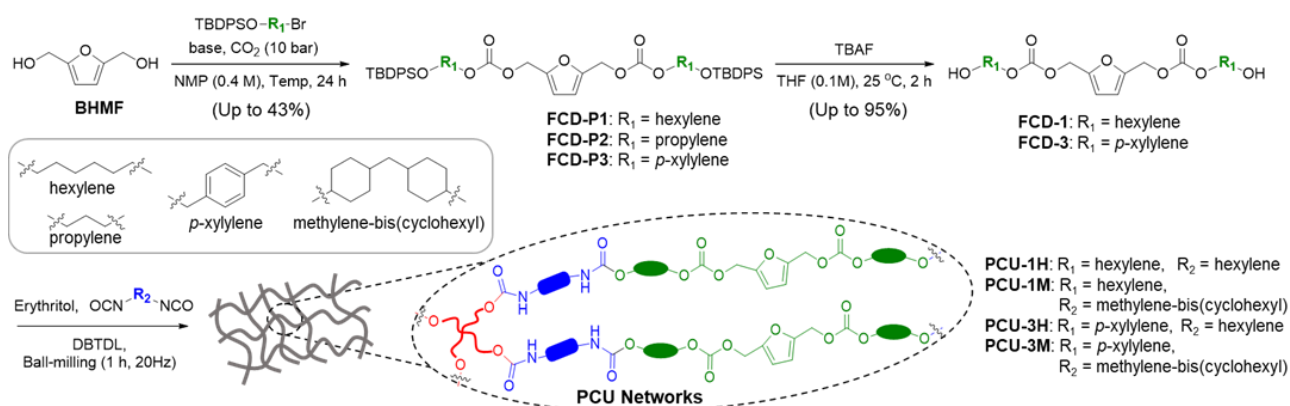
A 1A Retsch Mixer Mill MM 400 system (Haan, Germany) was used for the ball-milling experiments with a 25 mL stainless steel vessel and two stainless steel balls with a diameter of 15 mm each. The autoclave experiments employing a 50 mL stainless steel vessel were used as a system for applying pressure. Proton ( $^1\text{H}$ ) NMR spectra were recorded using a Bruker 500 MHz spectrometer (MA, USA). Carbon ( $^{13}\text{C}$ ) NMR spectra were recorded using a 125 MHz spectrometer with complete proton decoupling. The chemical shifts were reported in ppm ( $\delta$ ) with TMS as the internal standard; the coupling constants ( $J$ ) were expressed in Hz. Column chromatography was carried out using a 100–200-mesh silica gel. Thin-layer chromatography analysis was performed on precoated silica gel 60  $F_{254}$  slides (Merck, Darmstadt, Germany) and visualized by ultraviolet irradiation. Fourier transform infrared (FTIR) spectra were obtained using a spectrometer (Vertex70, Bruker Optics, MA, USA) equipped with a diamond attenuated total reflectance unit. The decomposition temperature ( $T_d$ ) of the polymer was determined by thermogravimetric analysis (TGA) using a Seiko Exstar 6000 (TG/DTA6100, Chiba, Japan). The measurements were carried out from 0 °C to 800 °C at a heating rate of 10 °C  $\cdot$  min $^{-1}$  under a flow of 100% nitrogen ( $\text{N}_2$ ). Differential scanning calorimetry (DSC) of the network powder was conducted using a DSC 7020 (Hitachi High-Tech, Tokyo, Japan) in temperatures ranging from –30 °C to 185 °C, 185 °C to –30 °C, and –30 °C to 185 °C with a heating/cooling rate of 5 °C  $\cdot$  min $^{-1}$ . The thermomechanical properties of films were characterized by dynamic mechanical analysis (DMA), which was carried out using a Seiko Exstar 6000 (DMA/SS6100, tension film mode). The temperature range was between –20 °C and 180 °C. The heating rate was 3 °C  $\cdot$  min $^{-1}$  at a 1 Hz frequency. Rheological measurements of films were carried out using the 25-mm-diameter parallel plates of a modular compact rheometer (MCR 302e, Anton Paar, Graz, Austria). Stress–relaxation experiments were performed over a temperature range of 140 °C to 160 °C at a 3% strain, and the relaxation modulus was monitored as a function of time. A constant normal force of 5 N was applied to ensure good contact with the plate. Samples were held at the measurement temperature for 10 min at regular intervals. Tensile analyses were conducted at a tensile rate of 3 mm  $\cdot$  min $^{-1}$  using a universal

testing machine (UTM) (34SC-05, Instron, Norwood, MA, USA). The UTM samples were prepared on a stainless steel plate (5 × 50 mm, 0.8 mm thickness) in a hot press at 120 °C for 6 h. Thermomechanical Analysis (TMA) (TMA6100, Chiba, Japan) was measured at 3 °C·min<sup>-1</sup> from -35 °C to 200 °C for additional healing properties measurement. TMA samples (3 × 20 mm, 0.8 mm thickness) were prepared in the same way as UTM.

### 3. Results

#### Synthesis of CO<sub>2</sub>-Immobilized Platform FCDs

The biomass-derived, CO<sub>2</sub>-immobilized platform FCDs were synthesized from biomass-derived diol BHMf via carbonation followed by a one-pot substitution reaction with a protected ω-hydroxy bromoalkane of three different moieties. The protected ω-hydroxy bromoalkanes (TBDPSO-R<sub>1</sub>-Br, P1~3) were prepared from an α,ω-dihydroxy alkane via bromination and silyl ether formation, or silyl ether protection on a ω-hydroxy-α-bromoalkane (Table S1). When CO<sub>2</sub> was pressurized (10 bar) in an autoclave reactor containing BHMf and TBDPSO-R<sub>1</sub>-Br in the presence of a base, CO<sub>2</sub> was successfully immobilized to BHMf with moderate yields (Scheme 1 and Table 1).



**Scheme 1.** Synthesis of the PCU networks from CO<sub>2</sub>-immobilized, biomass-derived carbonate diols (FCDs).

**Table 1.** Optimizing conditions for the synthesis of CO<sub>2</sub>-immobilized carbonate diol FCD-Ps<sup>1</sup>.

Entry	R <sub>1</sub>	Base	Temp.	Yield <sup>2</sup>
1	hexylene (2 eq)	DBU	80 °C	No reaction
2	hexylene (2 eq)	K <sub>2</sub> CO <sub>3</sub>	80 °C	20% <sup>3</sup>
3	hexylene (2 eq)	Cs <sub>2</sub> CO <sub>3</sub>	80 °C	17%
4	hexylene (2.2 eq)	Cs <sub>2</sub> CO <sub>3</sub>	80 °C	25% (29% <sup>4</sup> )
5	hexylene (2.2 eq)	Cs <sub>2</sub> CO <sub>3</sub>	100 °C	43%
6	propylene (2.2 eq)	Cs <sub>2</sub> CO <sub>3</sub>	100 °C	53%
7	p-xylylene (2.2 eq)	Cs <sub>2</sub> CO <sub>3</sub>	100 °C	8%

<sup>1</sup> Reaction and condition: BHMf (0.2 mmol), base (4.0 eq), NMP (0.4 M) using an autoclave under 10 bar CO<sub>2</sub>.

<sup>2</sup> Isolated yield. <sup>3</sup> NMR yield. <sup>4</sup> 48 h reaction.

We set out to optimize the synthetic conditions for the direct introduction of CO<sub>2</sub> using hexylene bromide P1 by screening bases using 8-diazabicyclo(5.4.0)undec-7-ene (DBU), potassium carbonate (K<sub>2</sub>CO<sub>3</sub>), and Cs<sub>2</sub>CO<sub>3</sub> (Table 1 entries 1–3). The reaction did not proceed with DBU and the starting materials remained mostly (entry 1). Only 20% conversion was observed in the <sup>1</sup>H-NMR analysis in the case of K<sub>2</sub>CO<sub>3</sub> (entry 2). The reaction conversion with respect to BHMf was significantly higher (90%) when Cs<sub>2</sub>CO<sub>3</sub> was used; however, the isolated yield was only 17% (entry 3). The isolated yield was marginally improved by increasing the equivalent bromide (entry 4) or lengthening the reaction time from 24 to 48 h (entry 4). For a higher yield, the reaction temperature was increased to 100 °C, resulting in a moderate yield of 43% at 24 h (entry 5). Other bromoalkanes (propylene P2 and xylylene P3) were also subjected to the optimized conditions, and the

corresponding protected carbonate diols (FCD-Ps) were obtained in isolated yields of 53% and 8%, respectively (entries 6 and 7). The yield in the case of *p*-xylylene bromide P3 was unsatisfactory, and it appeared that benzylic bromides were not compatible with nucleophilic substitution by the carbonate intermediate, resulting from CO<sub>2</sub> addition to the cesium alkoxide [54], or because unknown side reactions occurred.

The target FCDs were obtained through deprotection of FCD-Ps using TBAF (Scheme S1); however, only FCD-1 and FCD-3 were successfully isolated in yields up to 95%. In the case of FCD-2, which had a propylene group, it was confirmed by <sup>1</sup>H-NMR that a cyclic reaction occurred during deprotection, and propylene carbonate was produced as a by-product. Although the overall yields were only moderate, it should be noted that an ecofriendly polymer platform was successfully prepared by directly introducing CO<sub>2</sub> into a biomass-derived diol.

With FCDs at hand, the synthesis of biomass-derived PCU networks was attempted via a facile, ecofriendly mechanochemical method. Following the optimized conditions described elsewhere [52], a mixture including FCD, mesoerythritol, and diisocyanate (HDI or HMDI) was subjected to vibration ball-milling (20 Hz, 60 min) and subsequently hot-pressed (120 °C, 6 h, 30 MPa) to form urethane-bond networks (PCUs, Figure 1 and Table 2). The starting mixture comprised a ratio of diol:polyol(tetra-ol):diisocyanate = 1:1:3, which corresponded to the stoichiometric balance of [OH] and [NCO]. As shown in the PCU-1M spectra in the FTIR measurements (Figure 2a), immediately after the initial ball-milling, the portions of NCO moieties remained, suggesting that the reaction did not proceed completely, presumably because of an insufficient encountering of functional groups in the solid-state conditions. The NCO peak did not disappear, even when the ball-milling reaction was carried out for 2 h or more. These remainders became additional reaction sites during the hot-pressing. In fact, in the FTIR spectra, the stretching vibration of the NCO peak at 2262 cm<sup>-1</sup> disappeared completely in the PCU-1M film, and the sharp peaks at 1725 and 1246 cm<sup>-1</sup> were observed as emanating from the stretching vibrations of the urethane bond, C=O, and N–H, respectively. Additionally, the broad peaks at 3344 cm<sup>-1</sup> were shown by N–H stretching vibrations. The stretching vibrations of C=O in the FTIR spectra of urethane polymers can form two peaks: the free C=O and the hydrogen bonded C=O. Since the hydrogen bonding to C=O may weaken the double bond character, the peak for C=O stretching can shift to a lower wavenumber than that of free C=O [55]. When the FTIR spectra of PCU-1M prepolymer and hot-pressed film in the range of wavenumbers 1600–1800 cm<sup>-1</sup> were enlarged (Figure 2a), two peaks of C=O stretching were clearly presented. It can be assigned that the free C=O appears at 1742 cm<sup>-1</sup> and the hydrogen bonded C=O appears at 1700 cm<sup>-1</sup>. Interestingly, the portions of the hydrogen bonded C=O appeared to increase in the hot-pressed film, which can be attributed to the fact that under hot pressing conditions, more urethane bonds are formed and polymer chains can be rearranged for more hydrogen bonding. Other PCU and PCU films also showed similar patterns to PCU-1M as a result of FTIR measurements (Figure S1).

**Table 2.** Physical properties of synthesized PCUs as different types of alcohol and isocyanate chains<sup>1</sup>.

Entry	Alcohol (R <sub>1</sub> )	Isocyanate (R <sub>2</sub> )	T <sub>g</sub> <sup>2</sup> (°C)	T <sub>g</sub> <sup>3</sup> (°C)	T <sub>d5%</sub> <sup>4</sup> (°C)	T <sub>dmax</sub> <sup>5</sup> (°C)	tan δ	E' <sup>6</sup> (MPa)	T <sub>v</sub> <sup>7</sup> (°C)
PCU-1H	FCD-1	HDI (H)	38	12	210	490	0.35	4.2	104
PCU 1M	FCD-1	HMDI (M)	68	67	222	490	0.70	2.4	72
PCU-3H	FCD-3	HDI (H)	46	14	190	490	0.52	122	118
PCU-3M	FCD-3	HMDI (M)	60	69	220	490	0.60	0.54	65

<sup>1</sup> Conditions: alcohol (FCD-1 or FCD-3, 1.0 eq), erythritol (1.0 eq), isocyanate (HDI or HMDI, 3.0 eq), DBTDL (1.0 mol%) using ball-milling 20 Hz for 60 min. <sup>2</sup> Defined as the temperature of the maximum in tan δ. <sup>3</sup> Determined by DSC for the first cooling range from 185 °C to −30 °C at a heating rate of 5 °C·min<sup>-1</sup>. <sup>4</sup> Determined by the 5% weight-loss temperature from TGA. <sup>5</sup> Determined by the maximum temperature for fully degradation from TGA. <sup>6</sup> Determined by the rubbery plateau region in DMA curves. <sup>7</sup> Calculated using the Maxwell model and Arrhenius equation.

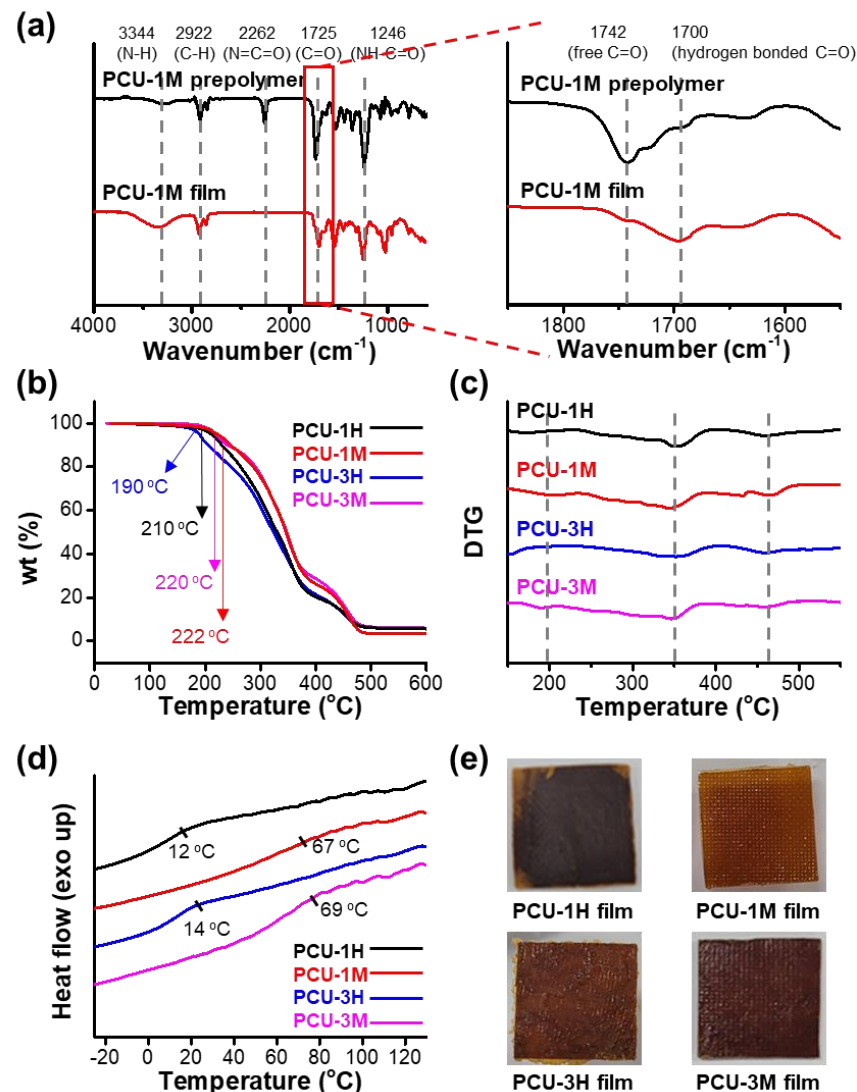


**Figure 2.** (a) Fourier transform infrared analysis of the PCU-1M prepolymer powder and the hot-pressed film, showing the complete conversion of the starting materials; (b) The TGA curves of films; (c) The DTG curves of the PCU films; (d) The DSC curves of the PCU films and the corresponding  $T_g$ s; (e) Photographs of the PCU films after the hot-pressing process.

We observed the swelling behavior of PCUs for up to 72 h in common laboratory solvents such as DMF, DMSO, and toluene (Figure S2). We observed that the swelling ratios of PCUs were very little in toluene (a few %), but relatively large in DMF and DMSO (up to 210%). Interestingly, hexylene-based PCU-1s showed the larger swelling ratios than p-xylylene-based PCU-3s; FCD moieties in PCUs seem to have more effect on swellings than diisocyanate parts. In addition, the dry weight after 72 h of swelling were measured, giving rise to a soluble fraction ( $f_{\text{soluble}}$ ). In fact, we observed the  $f_{\text{soluble}}$  of 2~41% of PCUs, which may suggest the portions of the incompletely crosslinked moieties. However, most of the masses (59~98%) appeared to remain after the swelling, which indicates that PCUs mostly have a good crosslinking network.

The film-production conditions were optimized through several trials to produce uniform films, thereby ensuring that all the starting materials were converted through the hot-press conditions (Figure 2e). As described above, the reaction did not proceed completely in the prepolymer state. The first step was to prepare a homogeneous state; the synthesized pre-PCU powder was dissolved in DMSO (10 wt%). The mixture was then transferred to a PTFE Teflon mold (30  $\times$  30 mm) and dried in an oven (70  $^{\circ}\text{C}$ ) for

12 h. The fabricated prefilm was placed in a stainless steel mold (30 × 5 mm, 0.8 mm thickness) and pressed for 6 h at 120 °C under a pressure of 30 MPa. Since pre-PCU powders synthesized with HMDI (PCU-Ms) were mixed homogeneously, the resulting films were also uniform during the hot press. However, pre-PCU powders made from HDI (PCU-Hs) did not dissolve or disperse well in the solution, and as a result, the film formation had to be performed in a rather heterogeneous state. Accordingly, slightly incongruent films were produced, presumably because the heat was not evenly distributed during the film formation.

Thermal properties of the CO<sub>2</sub>-immobilized, biomass-based PCU network polymers were tested through TGA and DSC (Figure 2b–d). For the TGA measurements, the samples were heated under an N<sub>2</sub> atmosphere at 10 °C·min<sup>−1</sup>, and the T<sub>d5%</sub> was defined at the point where the 5% weight loss occurred. As shown in Figure 2b, the T<sub>d5%</sub>s were in the range of 190 °C–222 °C, and the pattern of weight loss appeared to be very similar for all the PCUs. We attributed the initial weight loss of 15%–20% at approximately 200 °C to the decomposition of the bis(oxymethyl)furan moiety, which had the lowest thermal stability [51]. Next, the second loss at nearly 230 °C means the carbamate and carbonate decompositions. The weight loss after 400 °C can be attributed to the thermal reduction of the diisocyanate parts (Figure 2c). Furthermore, the shapes of the TGA profiles were dependent on the structure of the diisocyanate moieties; HMDI-based PCU-Ms showed slightly higher thermal stability compared with HDI-based PCU-Hs.

The glass transition temperature (T<sub>g</sub>) of the PCU networks was measured during the first cooling range from 185 °C to −30 °C at a rate of 5 °C·min<sup>−1</sup> (Figure 2d). The HDI-based PCUs, such as PCU-1H and PCU-3H, showed lower T<sub>g</sub>s (12 °C and 14 °C, respectively) compared with the HMDI-based PCUs, e.g., PCU-1M and PCU-3M (67 °C and 69 °C). The bis(cyclohexyl) segments in HMDI appeared rather torsionally rigid and there was reduced rotational freedom in the main chain, thereby increasing the T<sub>g</sub> [56]. However, despite torsional rigidity, PCU-Ms produced a more homogeneous state under hot-press conditions compared with PCU-Hs (see above), resulting in films that were mechanically more intact.

Thermomechanical properties were investigated using films from CO<sub>2</sub>-immobilized biomass-based PCU networks, which revealed their malleable and self-healing properties (Table 2 and Figure 3). The PCUs were fabricated into a 30 × 5 mm film (0.8 mm thickness) and characterized by DMA with the tension mode (heating rate 3 °C·min<sup>−1</sup>, 1% strain, and 1 Hz vibration) (Figure 3a). As the temperature increased from −20 °C to 180 °C, the tensile storage modulus (E′) of PCU-1H and PCU-1M was initially maintained at 4.2 and 827 MPa, respectively, until it began decreasing at ~38 °C and 68 °C, respectively. Here, T<sub>g</sub> was estimated to be the peak in tan δ (loss modulus E″/storage modulus E′). The difference in the T<sub>g</sub> of PCU-1s was attributed to the difference in the isocyanate moieties; the PCU based on the torsionally rigid HMDI showed a higher T<sub>g</sub>, which was consistent with the trends indicated by the DSC measurements above. Similarly, this trend was observed in PCU-3H and PCU-3M (46 °C and 60 °C, respectively). Interestingly, the initial E′ seems to depend largely on the FCD components; the aromatic group-containing FCD-3 resulted in higher E′ values (2.5 and 1.5 GPa for PCU-3H and PCU-3M, respectively) compared with linear alkyl FCD-1 (0.38 and 0.83 GPa for PCU-1H and PCU-1M, respectively). Furthermore, HMDI-based PCU-Ms showed larger drops in E′ at above their T<sub>g</sub> than HDI-based PCU-Hs (up to 2500 vs. 820 MPa). We suspected that in the flexible and elongated states above the T<sub>g</sub>, the interchain interactions arising from the linear alkyl groups in PCU-Hs tended to be stronger than those from the bis(cyclohexyl) groups in PCU-Ms.

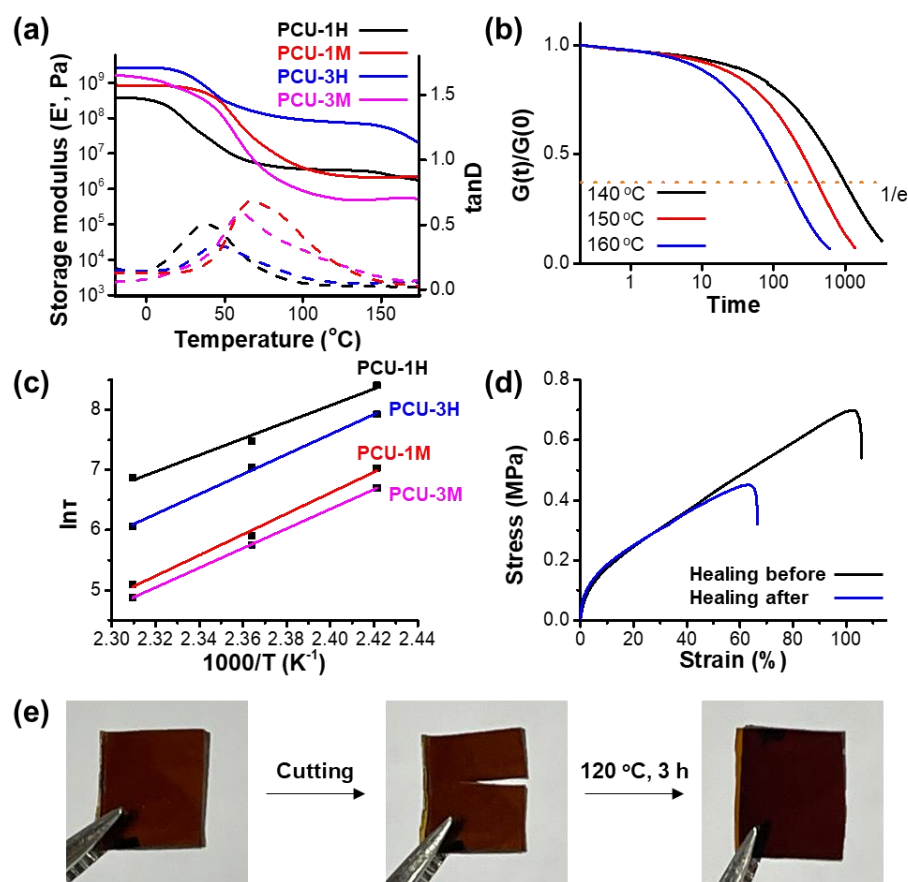


**Figure 3.** Thermomechanical properties of PCU films. (a) Tensile storage modulus and dissipation factor  $\tan \delta$ , measured using DMA from  $-20\text{ }^{\circ}\text{C}$  to  $180\text{ }^{\circ}\text{C}$  under an  $\text{N}_2$  atmosphere at a heating rate of  $3\text{ }^{\circ}\text{C}\cdot\text{min}^{-1}$ . (b) Normalized stress–relaxation curves as a function of time for three different isothermal temperatures from  $140\text{ }^{\circ}\text{C}$  to  $160\text{ }^{\circ}\text{C}$ . (c) Fitting of the relaxation times ( $\tau$ ) to the Arrhenius equation (see Supplementary Materials). (d) Tensile stress–strain curves before and after healing measured by UTM using the PCU-1M film. (e) Photographs showing thermal repairing of the cutted film of PCU-1M ( $120\text{ }^{\circ}\text{C}$ , 3 h).

After a decrease in the  $E'$ , the  $E'$  of HDMI-based PCU films (PCU-1M and PCU-3M film) maintained a rubbery plateau at above  $\sim 140\text{ }^{\circ}\text{C}$ . These plateaus suggested that the crosslinking density had been well-maintained and that the urethane (or carbonate) bond exchange may also have occurred as the temperature increased. Conversely, the  $E'$  of HDI-based PCU films (PCU-1H and PCU-3H film) showed a tendency to decrease at  $150\text{ }^{\circ}\text{C}$  or higher; accordingly, it was inferred that the crosslinking density may have decreased. We suspect that the decrease in  $E'$  of the PCU-Hs at extremely elevated temperatures had partly been due to the mechanically less-intact state of the HDI-based PCU films.

Stress–relaxation analyses were conducted to derive the dynamic covalent characteristics of the PCU networks. The sample sizes were  $5 \times 5\text{ mm}$  ( $0.8\text{ mm}$  thickness), and the shear storage modulus ( $G'$ ) was monitored from  $140\text{ }^{\circ}\text{C}$  to  $160\text{ }^{\circ}\text{C}$  ( $10\text{ }^{\circ}\text{C}$  intervals) while applying 3% strain and a constant normal force of 5 N as a function of time (Figure 3b). The normalized shear storage modulus [ $G(t)/G(0)$ ] was plotted as a function of the relaxation time ( $t$ ), and the representative stress–relaxation profiles for the rest of the PCU films are shown in Figure S3 and Table S2. According to the Maxwell relationship [ $G(t)/G_0 = \exp(-t/\tau^*)$ ], the characteristic relaxation time ( $\tau^*$ ) can be regarded as the time when the normalized modulus becomes a value of  $1/e$  ( $\approx 0.37$ ) [57–59]. When examining  $\tau^*$  at each temperature ( $T$ ), these may exhibit Arrhenius behavior, a characteristic of typical associative CANs or vitrimers. By fitting  $\ln \tau^*$  vs.  $1000/T$  according to the Arrhenius equation, the

kinetic activation energy ( $E_a$ ) can be obtained from the slopes of linear equation (Figure 3c). Using the relationship of viscosity ( $\eta$ ) and  $\tau^*$ , topology freezing transition temperature ( $T_v$ ) was also calculated by the slope of the trend line. The  $T_v$  is a key transition temperature in CANs (refer to the calculation procedure of the Supplementary Materials). At the  $T_v$ , the polymer network changes from a vitrified state to a deformable solid by a covalent-bond exchange reaction.

It seemed that the  $T_v$  of the PCU networks was largely determined by the diisocyanate moieties. The  $T_v$ s of HDI-based PCU-Hs were much higher (104 °C–118 °C) than those of HMDI-based PCU-Ms (65 °C–72 °C). The difference in  $T_v$ s appeared unclear because the same exchange reactions should have occurred in all PCUs; however, we suspect that the less-strong interchain interactions in PCU-Ms may have allowed for the faster exchange reactions. It should be noted that the dynamic bond exchange reactions in PCUs were clearly demonstrated by the rubbery plateaus in DMA and by the temperature-dependent stress–relaxation. Furthermore, it was shown that the thermomechanical properties of PCUs could be tuned via the choice of molecular structures in diol or diisocyanate moieties.

Based on the dynamic bond exchanges in PCUs, the self-healing properties of PCU-1M films were investigated through tensile testing using a UTM (Figure 3d,e). The PCU-1M film before healing was flexible and reflected a strain capacity of above 100% and tensile strength of 0.71 MPa. A portion of the PCU-1M film was cut and cured at 120 °C for 3 h to obtain a fully cured film (Figure 3e). This cured film showed a healing efficiency of approximately 60% (a recovered tensile strength of 0.43 MPa). In addition, performance measurement before and after healing was additionally measured using TMA, showing the original thermomechanical property was restored (Figure S4).

Although a dynamic bond exchange reaction was demonstrated in PCUs, it is not clear whether transcarbamoylation (i.e., urethane exchange) or transcarbonation (i.e., carbonate exchange) occurred, or whether both reactions occurred simultaneously. To investigate which reaction occurred predominantly, we investigated the reactivity of the exchange reactions through a model-compound study using gas chromatography (GC) analysis (Figure 4). For the model exchange reactions, phenyl and toluene-functionalized carbamates (U1–4) and carbonates (C1–4) were synthesized with hexyl and propyl groups (each in  $2 \times 2 = 4$  combinations). The exchange reactions were performed by combining model molecules in the presence of DBTDL at 120 °C. The reaction conditions were the same for the PCU synthesis, except that the reaction was performed in acetonitrile (ACN, ~33 mM). First, to check the exchange reactivity between carbonates, C1 and C2 were combined and the reaction proceeded for 12 h, resulting in no change in GC profiles (Figure 4a). When C1 and U2 were mixed and tested for the reactivity between carbonate and carbamate, the starting materials remained after the reaction and no product was found (Figure 4b). However, when carbamates U1 and U2 were combined, the reaction proceeded, and it was confirmed that the exchange products, U3 and U4, had been generated (Figure 4c). Therefore, evidence showed that the exchange reaction may occur only between carbamates (urethanes) in PCU networks, and could be responsible for the covalent adaptive characteristics.

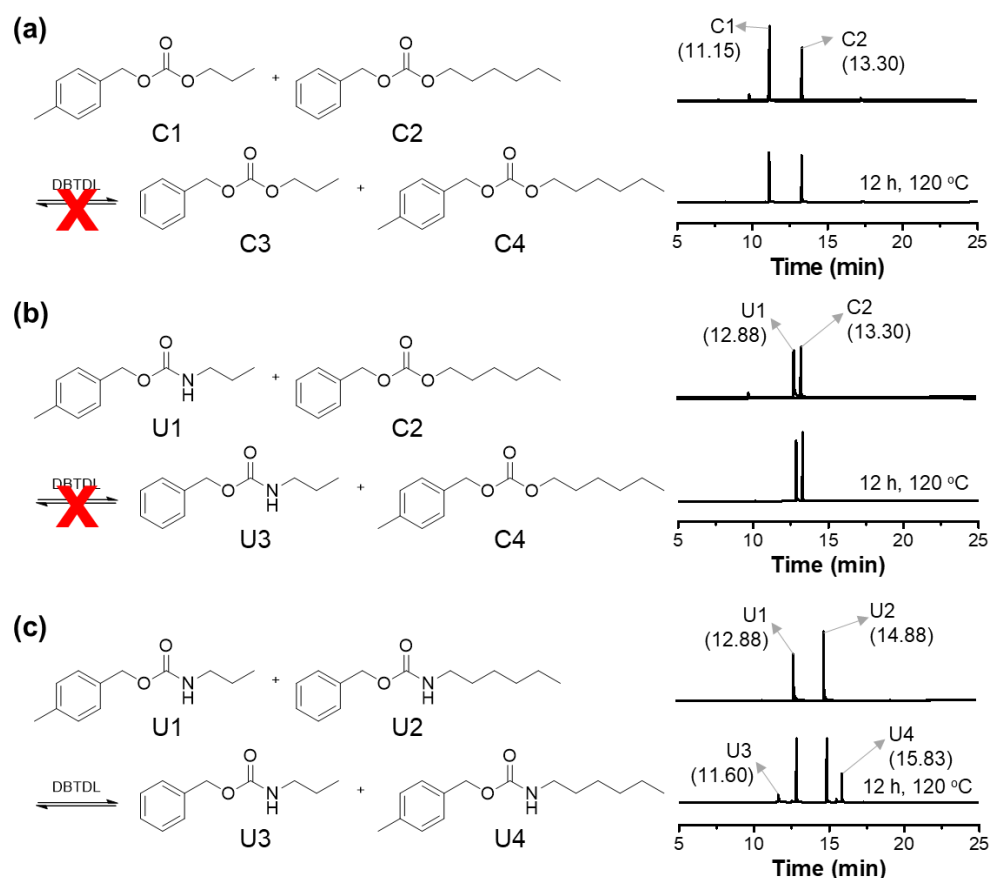


**Figure 4.** GC analyses during the exchange reactions (transcarbonation or transcarbamoylation) using the model compounds. (a) Exchange between carbonates (C1 + C2), resulting in no reaction. (b) Exchange between the carbonate and carbamate (U1 + C2), showing no change. (c) Exchange between carbamates (U1 + U2), and the appearance of new carbamates (U3 and U4).

#### 4. Conclusions

In summary, a new CO<sub>2</sub> utilization strategy was suggested, and FCDs were successfully synthesized by introducing CO<sub>2</sub> directly into a biomass-derived diol BHMf. Using FCDs, PCU networks were prepared with erythritol and diisocyanate in a ratio of [OH]:[NCO] = 1:1 via facile ball-milling. The thermal and thermomechanical properties of PCUs were thoroughly investigated using TGA, DMA, and rheometry, and revealed the characteristics in the form of a CAN. It was shown that the molecular structures of FCDs (hexylene or *p*-xylylene) and diisocyanates (hexylene or (bis)cyclohexyl) affected the glass transition temperature, topology freezing temperature, and the rubbery storage modulus  $E'$ . In addition, the malleable, recyclable, and healable properties of the biomass-derived, CO<sub>2</sub>-immobilized PCUs were demonstrated, which arose due to the dynamic bond exchange reactions. It was confirmed via a model compound study that the bond exchanges occurred mainly between carbamates (not carbonates) under the specific reaction conditions. We believe our strategy presents an efficient approach for using biomass and CO<sub>2</sub> simultaneously, and for producing sustainable polyurethanes and other copolymers.

**Supplementary Materials:** The following are available online at <https://www.mdpi.com/article/10.3390/polym13244381/s1>, T<sub>v</sub> Calculations method Table S1: Synthesis of TBDPSO-R<sub>1</sub>-Br, Table S2: SRA of PCU-1H, PCU-3H and PCU-3M films, Scheme S1: Optimizing conditions for the deprotection of FCD-PS, Figure S1: FTIR spectra of PCU-1H, PCU-3H, and PCU-3M in the prepolymer state and the film state, Figure S2: Swelling tests of PCU-1H, PCU-1M, PCU-3H, and PCU-3M, Figure S3: SRA of PCU-1H, PCU-3H, and PCU-3M through a rheometer, Figure S4: TMA of PCU-1M films before and after healing.

**Author Contributions:** Conceptualization, S.B., J.L., and C.S.; Methodology S.B., J.L., I.C. and H.K.; Writing–Review and Editing, S.B., J.L., and C.S. All authors have read and agreed to the published version of the manuscript.

**Funding:** This work was supported by “Next Generation Carbon Upcycling Project” (Project No. 2017M1A2A2043146) through the National Research Foundation (NRF) funded by the Ministry of Science and ICT, Republic of Korea. This research was also supported by the Civil-Military Technology Cooperation Center funded by the Defense Acquisition Program Administration and Ministry of Trade, Industry and Energy, Republic of Korea under grant No. 20-CM-BR-05.

**Institutional Review Board Statement:** Not applicable.

**Informed Consent Statement:** Not applicable.

**Data Availability Statement:** The data presented in this study are available on request from the corresponding authors.

**Conflicts of Interest:** The authors declare no conflict of interest.

## References

1. Sanz-Pérez, E.S.; Murdock, C.R.; Didas, S.A.; Jones, C.W. Direct capture of CO<sub>2</sub> from ambient air. *Chem. Rev.* **2016**, *116*, 11840–11876. [[CrossRef](#)] [[PubMed](#)]
2. Chen, Z.; Hadjichristidis, N.; Feng, X.; Gnanou, Y. Cs<sub>2</sub> CO<sub>3</sub>-promoted polycondensation of CO<sub>2</sub> with diols and dihalides for the synthesis of miscellaneous polycarbonates. *Polym. Chem.* **2016**, *7*, 4944–4952. [[CrossRef](#)]
3. Zhou, Q.; Gu, L.; Gao, Y.; Qin, Y.; Wang, X.; Wang, F. Biodegradable CO<sub>2</sub>-based polycarbonates with rapid and reversible thermal response at body temperature. *J. Polym. Sci. Part A Polym. Chem.* **2013**, *51*, 1893–1898. [[CrossRef](#)]
4. Kemper, J. Biomass and carbon dioxide capture and storage: A review. *Int. J. Greenh. Gas Control* **2015**, *40*, 401–430. [[CrossRef](#)]
5. Fang, M.; Yi, N.; Di, W.; Wang, T.; Wang, Q. Emission and control of flue gas pollutants in CO<sub>2</sub> chemical absorption system—A review. *Int. J. Greenh. Gas Control* **2020**, *93*, 102904. [[CrossRef](#)]
6. Zhang, F.; Liu, P.; Zhang, K.; Song, Q.-W. Chemical Adsorption Strategy for DMC-MeOH Mixture Separation. *Molecules* **2021**, *26*, 1735. [[CrossRef](#)]
7. Gui, X.; Tang, Z.; Fei, W. CO<sub>2</sub> capture with physical solvent dimethyl carbonate at high pressures. *J. Chem. Eng. Data* **2010**, *55*, 3736–3741. [[CrossRef](#)]
8. Grignard, B.; Gennen, S.; Jérôme, C.; Kleij, A.W.; Detrembleur, C. Advances in the use of CO<sub>2</sub> as a renewable feedstock for the synthesis of polymers. *Chem. Soc. Rev.* **2019**, *48*, 4466–4514. [[CrossRef](#)]
9. Hosseinian, A.; Farshbaf, S.; Mohammadi, R.; Monfared, A.; Vessally, E. Advancements in six-membered cyclic carbonate (1,3-dioxan-2-one) synthesis utilizing carbon dioxide as a C1 source. *RSC Adv.* **2018**, *8*, 17976–17988. [[CrossRef](#)]
10. Tamura, M.; Ito, K.; Honda, M.; Nakagawa, Y.; Sugimoto, H.; Tomishige, K. Direct copolymerization of CO<sub>2</sub> and diols. *Sci. Rep.* **2016**, *6*, 1–9. [[CrossRef](#)]
11. Gregory, G.L.; Ulmann, M.; Buchard, A. Synthesis of 6-membered cyclic carbonates from 1,3-diols and low CO<sub>2</sub> pressure: A novel mild strategy to replace phosgene reagents. *Rsc Adv.* **2015**, *5*, 39404–39408. [[CrossRef](#)]
12. Guo, L.; Zhang, R.; Xiong, Y.; Chang, D.; Zhao, H.; Zhang, W.; Zheng, W.; Chen, J.; Wu, X. The Application of Biomass-Based Catalytic Materials in the Synthesis of Cyclic Carbonates from CO<sub>2</sub> and Epoxides. *Molecules* **2020**, *25*, 3627. [[CrossRef](#)] [[PubMed](#)]
13. Thorat, S.D.; Phillips, P.J.; Semenov, V.; Gakh, A. Physical properties of aliphatic polycarbonates made from CO<sub>2</sub> and epoxides. *J. Appl. Polym. Sci.* **2003**, *89*, 1163–1176. [[CrossRef](#)]
14. Coates, G.W.; Moore, D.R. Discrete metal-based catalysts for the copolymerization of CO<sub>2</sub> and epoxides: Discovery, reactivity, optimization, and mechanism. *Angew. Chem. Int. Ed.* **2004**, *43*, 6618–6639. [[CrossRef](#)]
15. Darensbourg, D.J.; Wilson, S.J. What’s new with CO<sub>2</sub>? Recent advances in its copolymerization with oxiranes. *Green Chem.* **2012**, *14*, 2665–2671. [[CrossRef](#)]
16. Tiwari, A.; Titinchi, S. *Advanced Catalytic Materials*; John Wiley & Sons: Hoboken, NJ, USA, 2015.
17. Paul, S.; Zhu, Y.; Romain, C.; Brooks, R.; Saini, P.K.; Williams, C.K. Ring-opening copolymerization (ROCOP): Synthesis and properties of polyesters and polycarbonates. *Chem. Commun.* **2015**, *51*, 6459–6479. [[CrossRef](#)] [[PubMed](#)]
18. Trott, G.; Saini, P.; Williams, C. Catalysts for CO<sub>2</sub>/epoxide ring-opening copolymerization. *Philos. Trans. R. Soc. A Math. Phys. Eng. Sci.* **2016**, *374*, 20150085. [[CrossRef](#)]
19. Taherimehr, M.; Pescarmona, P.P. Green polycarbonates prepared by the copolymerization of CO<sub>2</sub> with epoxides. *J. Appl. Polym. Sci.* **2014**, *131*, 41141. [[CrossRef](#)]
20. Stille, J.K. Step-Growth Polymerization. *J. Chem. Educ.* **1981**, *58*, 862–866. [[CrossRef](#)]
21. Bian, S.; Pagan, C.; Andrianova “Artemyeva”, A.A.; Du, G. Synthesis of polycarbonates and poly (ether carbonate) s directly from carbon dioxide and diols promoted by a Cs<sub>2</sub>CO<sub>3</sub>/CH<sub>2</sub>Cl<sub>2</sub> system. *ACS Omega* **2016**, *1*, 1049–1057. [[CrossRef](#)]
22. Kadokawa, J.i.; Habu, H.; Fukamachi, S.; Karasu, M.; Tagaya, H.; Chiba, K. Direct polycondensation of carbon dioxide with xylylene glycols: A new method for the synthesis of polycarbonates. *Macromol. Rapid Commun.* **1998**, *19*, 657–660. [[CrossRef](#)]

23. Nettles, J.; Birks, P.; Sucre, E.; Bilby, R. Sustainable production of bioenergy feedstock from the industrial forest: Potential and challenges of operational scale implementation. *Curr. Sustain./Renew. Energy Rep.* **2015**, *2*, 121–127. [[CrossRef](#)]
24. Sacia, E.R.; Balakrishnan, M.; Bell, A.T. Biomass conversion to diesel via the etherification of furanyl alcohols catalyzed by Amberlyst-15. *J. Catal.* **2014**, *313*, 70–79. [[CrossRef](#)]
25. Dhillon, R.; von Wuehlisch, G. Mitigation of global warming through renewable biomass. *Biomass Bioenergy* **2013**, *48*, 75–89. [[CrossRef](#)]
26. de Haro, J.C.; Allegretti, C.; Smit, A.T.; Turri, S.; D'Arrigo, P.; Griffini, G. Biobased polyurethane coatings with high biomass content: Tailored properties by lignin selection. *ACS Sustain. Chem. Eng.* **2019**, *7*, 11700–11711. [[CrossRef](#)]
27. Xue, Z.; Ma, M.-G.; Li, Z.; Mu, T. Advances in the conversion of glucose and cellulose to 5-hydroxymethylfurfural over heterogeneous catalysts. *RSC Adv.* **2016**, *6*, 98874–98892. [[CrossRef](#)]
28. Lee, C.H.; Takagi, H.; Okamoto, H.; Kato, M. Improving the mechanical properties of isosorbide copolycarbonates by varying the ratio of comonomers. *J. Appl. Polym. Sci.* **2013**, *127*, 530–534. [[CrossRef](#)]
29. Maniar, D.; Jiang, Y.; Woortman, A.J.; van Dijken, J.; Loos, K. Furan-Based Copolyesters from Renewable Resources: Enzymatic Synthesis and Properties. *ChemSusChem* **2019**, *12*, 990. [[CrossRef](#)]
30. Zaldivar, J.; Nielsen, J.; Olsson, L. Fuel ethanol production from lignocellulose: A challenge for metabolic engineering and process integration. *Appl. Microbiol. Biotechnol.* **2001**, *56*, 17–34. [[CrossRef](#)]
31. Awuchi, C.G.; Echeta, K.C. Current developments in sugar alcohols: Chemistry, nutrition, and health concerns of sorbitol, xylitol, glycerol, arabitol, inositol, maltitol, and lactitol. *Int. J. Adv. Acad. Res.* **2019**, *5*, 1–33.
32. Kohli, K.; Prajapati, R.; Sharma, B.K. Bio-based chemicals from renewable biomass for integrated biorefineries. *Energies* **2019**, *12*, 233. [[CrossRef](#)]
33. Jeya, M.; Lee, K.-M.; Tiwari, M.K.; Kim, J.-S.; Gunasekaran, P.; Kim, S.-Y.; Kim, I.-W.; Lee, J.-K. Isolation of a novel high erythritol-producing *Pseudozyma tsukubaensis* and scale-up of erythritol fermentation to industrial level. *Appl. Microbiol. Biotechnol.* **2009**, *83*, 225–231. [[CrossRef](#)] [[PubMed](#)]
34. Hao, Q.; Li, F.; Li, Q.; Li, Y.; Jia, L.; Yang, J.; Fang, Q.; Cao, A. Preparation and crystallization kinetics of new structurally well-defined star-shaped biodegradable poly (L-lactide) s initiated with diverse natural sugar alcohols. *Biomacromolecules* **2005**, *6*, 2236–2247. [[CrossRef](#)]
35. Zhang, S.; Liu, T.; Hao, C.; Wang, L.; Han, J.; Liu, H.; Zhang, J. Preparation of a lignin-based vitrimer material and its potential use for recoverable adhesives. *Green Chem.* **2018**, *20*, 2995–3000. [[CrossRef](#)]
36. Schmidt, S.; Gatti, F.J.; Luitz, M.; Ritter, B.S.; Bruchmann, B.; Müllhaupt, R. Erythritol dicarbonate as intermediate for solvent- and isocyanate-free tailoring of bio-based polyhydroxyurethane thermoplastics and thermoplastic elastomers. *Macromolecules* **2017**, *50*, 2296–2303. [[CrossRef](#)]
37. Fridrihsone, A.; Stirna, U.; Lazdiņa, B.; Misāne, M.; Vilsone, D. Characterization of polyurethane networks structure and properties based on rapeseed oil derived polyol. *Eur. Polym. J.* **2013**, *49*, 1204–1214. [[CrossRef](#)]
38. Kausar, A. *Polyurethane/Epoxy Interpenetrating Polymer Network*; InTech: London, UK, 2017; Volume 10, pp. 1–16.
39. Zhang, Y.; Heath, R.; Hourston, D. Morphology, mechanical properties, and thermal stability of polyurethane–epoxide resin interpenetrating polymer network rigid foams. *J. Appl. Polym. Sci.* **2000**, *75*, 406–416. [[CrossRef](#)]
40. Atiqah, A.; Mastura, M.T.; Ahmed Ali, B.A.; Jawaid, M.; Sapuan, S.M. A review on polyurethane and its polymer composites. *Curr. Org. Synth.* **2017**, *14*, 233–248. [[CrossRef](#)]
41. Yang, X.; Guo, L.; Xu, X.; Shang, S.; Liu, H. A fully bio-based epoxy vitrimer: Self-healing, triple-shape memory and reprocessing triggered by dynamic covalent bond exchange. *Mater. Des.* **2020**, *186*, 108248. [[CrossRef](#)]
42. Altuna, F.I.; Pettarin, V.; Williams, R.J. Self-healable polymer networks based on the cross-linking of epoxidised soybean oil by an aqueous citric acid solution. *Green Chem.* **2013**, *15*, 3360–3366. [[CrossRef](#)]
43. Li, M.; Ding, H.; Yang, X.; Xu, L.; Xia, J.; Li, S. Preparation and properties of self-healing polyurethane elastomer derived from tung-oil-based polyphenol. *ACS Omega* **2019**, *5*, 529–536. [[CrossRef](#)] [[PubMed](#)]
44. Sheppard, D.T.; Jin, K.; Hamachi, L.S.; Dean, W.; Fortman, D.J.; Ellison, C.J.; Dichtel, W.R. Reprocessing postconsumer polyurethane foam using carbamate exchange catalysis and twin-screw extrusion. *ACS Cent. Sci.* **2020**, *6*, 921–927. [[CrossRef](#)]
45. Erice, A.; de Luzuriaga, A.R.; Matxain, J.M.; Ruipérez, F.; Asua, J.M.; Grande, H.-J.; Rekondo, A. Reprocessable and recyclable crosslinked poly (urea-urethane) s based on dynamic amine/urea exchange. *Polymer* **2018**, *145*, 127–136. [[CrossRef](#)]
46. Denissen, W.; Winne, J.M.; Du Prez, F.E. Vitrimers: Permanent organic networks with glass-like fluidity. *Chem. Sci.* **2016**, *7*, 30–38. [[CrossRef](#)]
47. Alraddadi, M.A.; Chiaradia, V.; Stubbs, C.J.; Worch, J.C.; Dove, A.P. Renewable and recyclable covalent adaptable networks based on bio-derived lipic acid. *Polym. Chem.* **2021**, *12*, 5796–5802. [[CrossRef](#)]
48. Khan, A.; Ahmed, N.; Rabnawaz, M. Covalent Adaptable Network and Self-Healing Materials: Current Trends and Future Prospects in Sustainability. *Polymers* **2020**, *12*, 2027. [[CrossRef](#)] [[PubMed](#)]
49. Lamm, M.E.; Song, L.; Wang, Z.; Lamm, B.; Fu, L.; Tang, C. A facile approach to thermomechanically enhanced fatty acid-containing bioplastics using metal–ligand coordination. *Polym. Chem.* **2019**, *10*, 6570–6579. [[CrossRef](#)]
50. Hu, J.; Mo, R.; Sheng, X.; Zhang, X. A self-healing polyurethane elastomer with excellent mechanical properties based on phase-locked dynamic imine bonds. *Polym. Chem.* **2020**, *11*, 2585–2594. [[CrossRef](#)]

51. Choi, E.H.; Lee, J.; Son, S.U.; Song, C. Biomass-derived furanic polycarbonates: Mild synthesis and control of the glass transition temperature. *J. Polym. Sci. Part A Polym. Chem.* **2019**, *57*, 1796–1800. [[CrossRef](#)]
52. Oh, C.; Choi, E.H.; Choi, E.J.; Premkumar, T.; Song, C. Facile Solid-State Mechanochemical Synthesis of Eco-Friendly Thermoplastic Polyurethanes and Copolymers Using a Biomass-Derived Furan Diol. *ACS Sustain. Chem. Eng.* **2020**, *8*, 4400–4406. [[CrossRef](#)]
53. Kim, H.; Cha, I.; Yoon, Y.; Cha, B.J.; Yang, J.; Kim, Y.D.; Song, C. Facile Mechanochemical Synthesis of Malleable Biomass-Derived Network Polyurethanes and Their Shape-Memory Applications. *ACS Sustain. Chem. Eng.* **2021**, *9*, 6952–6961. [[CrossRef](#)]
54. Oi, S.; Nemoto, K.; Matsuno, S.; Inoue, Y. Direct synthesis of polycarbonates from CO<sub>2</sub>, diols, and dihalides. *Macromol. Rapid Commun.* **1994**, *15*, 133–137. [[CrossRef](#)]
55. Cao, H.; Qi, F.; Liu, R.; Wang, F.; Zhang, C.; Zhang, X.; Chai, Y.; Zhai, L. The influence of hydrogen bonding on N-methyldiethanolamine-extended polyurethane solid–solid phase change materials for energy storage. *Rsc Adv.* **2017**, *7*, 11244–11252. [[CrossRef](#)]
56. Jiang, L.; Ren, Z.; Zhao, W.; Liu, W.; Liu, H.; Zhu, C. Synthesis and structure/properties characterizations of four polyurethane model hard segments. *R. Soc. Open Sci.* **2018**, *5*, 180536. [[CrossRef](#)]
57. Wright, K.J.; Badwaik, V.D.; Samaddar, S.; Hyun, S.-H.; Glauninger, K.; Eom, T.; Thompson, D.H. Organocatalytic synthesis and evaluation of polycarbonate pendant polymer:  $\beta$ -Cyclodextrin-based nucleic acid delivery vectors. *Macromolecules* **2018**, *51*, 670–678. [[CrossRef](#)]
58. Schoustra, S.K.; Dijkman, J.A.; Zuilhof, H.; Smulders, M.M. Molecular control over vitrimer-like mechanics–tunable dynamic motifs based on the Hammett equation in polyimine materials. *Chem. Sci.* **2021**, *12*, 293–302. [[CrossRef](#)]
59. Tellers, J.; Pinalli, R.; Soliman, M.; Vachon, J.; Dalcanale, E. Reprocessable vinylogous urethane cross-linked polyethylene via reactive extrusion. *Polym. Chem.* **2019**, *10*, 5534–5542. [[CrossRef](#)]